Supporting Information

*for Soft Matter, 2016, DOI: 10.1039/C6SM01151A*

# A Photocurable Leaky Dielectric Material for Highly Electrical Insulating Electrohydrodynamic Micro-/Nanopatterns

*Guolong Wang,*[†] *Guowei Lv,*[†] *Shihu Zhang,*[†] *Jinyou Shao,*[‡] *Xiangming Li,*[‡] *Hongmiao Tian,*[‡] *Demei Yu,**[,†] *and Lifeng Zhang**[,§]

[†]Department of Applied Chemistry, School of Science, State Key Laboratory of Electrical Insulation and Power Equipment, School of Electrical Engineering, and ‡Micro- and Nano-technology Research Center, State Key Laboratory of Manufacturing Systems Engineering, Xi'an Jiaotong University, Xi'an 710049, China

[§]Department of Nanoengineering, Joint School of Nanoscience and Nanoengineering, North Carolina A&T State University, Greensboro, NC 27401, USA

**Corresponding Author**

* E-mail: (D.Y.) dmyu@mail.xjtu.edu.cn.

* E-mail: (L. Z.) lzhang@ncat.edu

## 1. Experimental Section

Bisphenol A ethoxylate dimethacrylate (BPAEODMA) was purchased from Guangzhou Deco Composite Technology. Chloroform-soluble and BPAEODMA-compatible poly(N-(methacryl ethyl) pyrrole) (PMAEPy) ($M_n$ = 6500, polydispersity = 1.126) was synthesized in lab. Darocur 1173 (2-hydroxy-2-methyl-1-phenyl-1-propanone) was used as photo-initiator. Reagent grade chloroform was supplied by Shanghai Sinopharm Chemical Reagent Co. Ltd. Heptadecafluorodecyltrimethoxysilane ($CF_3(CF_2)_7CH_2CH_2Si(OCH_3)_3$, FAS) was purchased from SICONG Chemical. Highly polished *n*-doped silicon (Si) wafers with <111> crystal orientation and resistance of 0.002 - 0.005Ω·cm were obtained from MCL Electronic Materials, Ltd. and used as template electrode. Indium tin oxide (ITO)-coated glass slides with a resistance of 8 Ω·cm were used as transparent substrates for in situ optical observation and UV light transmittance. Polyimide (PI) films with different thickness were purchased from 3M Company and used as spacer in the process of EHDP patterning.

A series of photocurable leaky dielectric material systems (the weight ratio of BPAEODMA/chloroform/1173 is 30/70/6) with $\varphi_{P/B}$ (the weight ratio of PMAEPy to BPAEODMA) of 0.00, 0.01, 0.02, 0.03, 0.04 and 0.05 were prepared by mixing the BPAEODMA and 1173 with the solution chloroform of PMAEPy. The experimental setup for EISF under flat electrodes started with spin-coating of the prepared material into a thin film with thickness $h$ = 13 μm on a silicon wafer substrate as one electrode and then a transparent ITO-coated glass template as second electrode was placed at a

certain distance $d$ = 28 μm leaving a small air gap. Following this step, a DC electric voltage $U$ = 200 V was applied between the template and substrate, the prepolymer surface deformed as the amplification of the capillary surface instability for the thin film. Finally, the deformation caused the formation of liquid bridges between the two capacitor plates, then with the voltage still applied the patterns were photocured by exposure to a UV lamp (MEJIRO PRECISION SHG-20) with wavelength of 253.7 nm and turned into perfect dielectric pillars. As for DEP-ECF DI process, a silicon template with microhole array was initially brought into proper contact with the surface of pre-polymer film that have been coated on ITO/glass substrate by a small pressure (0.1 $kg \cdot cm^{-2}$) and then kept at a fixed position ($h$ = 25μm) relative to the substrate. The Si template was also thermally dry-oxidized to grow a dielectric layer of $SiO_2$ with a thickness of 300 nm. The back layer of $SiO_2$ was chemically etched away with Hydrofluoric acid to expose the silicon for use as an electrode. Next, a square-wave voltage of 200 $V_{pp}$ with 10 Hz was applied between the template and substrate and sustained for 20 s before the curing step, pulling the liquid pre-polymer into template cavities. The voltages in this experment were generated with an arbitrary waveform generator (AGILENT 33220A) in conjunction with a highvoltage/amplifier/controller (TREK 610E). After the solidification and demolding step, the duplicated patterns were obtained. Note that all the templates were pre-treated by FAS as previously described to ease the demolding process.[1]

Steady rheology of the prepared material systems were characterized by a rotational rheometer (MCR302, Anton Paar Germany) with cone-plate system (C50-1) at 30 °C. Surface tension and contact angle of the prepared material systems were measured on a Dataphysics OCA20 system at ambient temperature. Dielectric properties of the prepared material systems and their corresponding cured film were measured by using NOVOCONTROL Concept 80 broadband dielectric spectrometer. Electrical breakdown strength of the corresponding solidified film (75 ± 8 μm) was measured using a breakdown voltage instrument (HUAYANG INSTRUMENT HJC-100KV) by sweeping the applied voltage from 3.4 KV (AC/50Hz) at approximately 1 KV/s until a sharp current increase was observed in transformer oil at ambient temperature. Fracture surface morphologies of the cured PMAEPy/BPAEODMA film were examined by JEOL JSM 7000F SEM. The SEM images and 3D images of EHDP structures were obtained by a HITACHI S-3000N SEM and LSCM (Olympus OLS4000), respectively.

## 2. The Dielectric Properties of Solidified PMAEPy/BPAEODMA Films

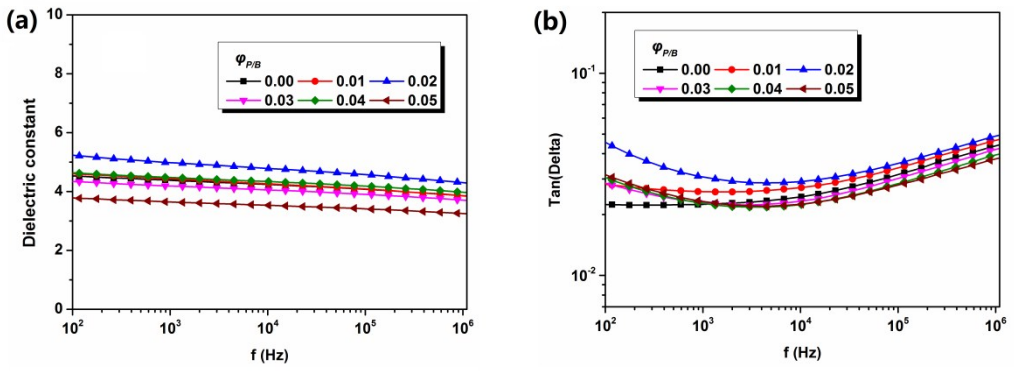


**Figure S1.** The dielectric properties of solidified PMAEPy/BPAEODMA films

## 3. The Influence of PMAEPy Content on Characteristic Wavelength $\lambda$ and Processing Time Scale of EISF Patterns

With the increase of PMAEPy content from $\varphi_{P/B} = 0$ to $\varphi_{P/B} = 0.05$, the experimental $\lambda$ (namely statistical average of the distance between the centers of adjacent pillars) gradually reduced from 325.6 ± 14.7 μm to 154.5 ± 15.3 μm, as shown in Figure S2 and Figure S3(a).

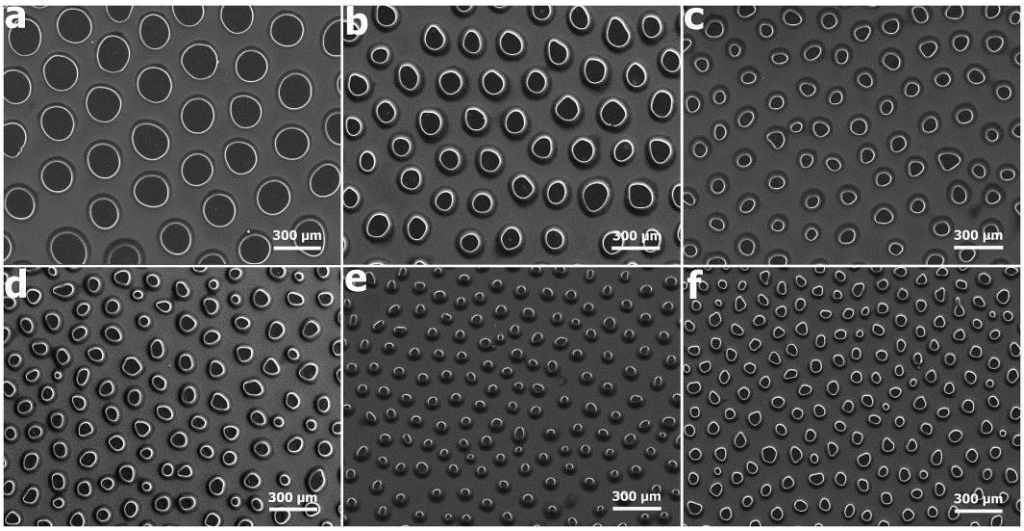


**Figure S2.** SEM images of EISF patterns of the films which were derived from PMAEPy/BPAEODMA material systems at varied ratios: (a) $\varphi_{P/B} = 0.00$; (b) $\varphi_{P/B} = 0.01$; (c) $\varphi_{P/B} = 0.02$; (d) $\varphi_{P/B} = 0.03$; (e) $\varphi_{P/B} = 0.04$; (f) $\varphi_{P/B} = 0.05$. Experimental conditions: $h = 13$ μm, $d = 28$ μm, $f = 0.464$, $U = 200$V.

The EHDP material system with $\varphi_{P/B} = 0$ behaves more like perfect dielectric, which is consistent with its low conductivity around $10^{-9}$ S/cm. Based on the perfect dielectric model in which the electrostatic stress at polymer layer-air interface is caused only by polarization effects [or dielectric pressure $p_D$, as illustrated in Figure S3(b-i)], linear stability analysis predicts a characteristic wavelength $\lambda$, which corresponds to the spacing between patterned pillars, with the fastest linear growth rate in a homogeneous electric field,[2,3]

$$\lambda_{\max} = \frac{2\pi}{U}\sqrt{\frac{2\gamma[\varepsilon_p d - (\varepsilon_p - 1)h]^3}{\varepsilon_0 \varepsilon_p (\varepsilon_p - 1)^2}} \quad (1)$$

where $\gamma$ is the surface tension of the film, $\varepsilon_0$ and $\varepsilon_p$ the dielectric constant of vacuum and polymer film, respectively. According to Equation 1, the theoretical $\lambda$ of perfect dielectric material ($\varphi_{P/B} = 0$) under current experimental condition is 368 μm, which is slightly larger than the experimental $\lambda$ (325.6 ± 14.7 μm). As for the EHDP material system containing PMAEPy ($\varphi_{P/B} \geq 0.01$), free charges at polymer-air interface have to be taken into consideration due to their high conductivity, i.e., up to ~$10^{-5}$ S/cm when $\varphi_{P/B} = 0.05$. Leaky dielectric model has been proposed to account for the free charge at polymer layer-air interface.[3,4] The accumulation of free charges at the interface abates electric field inside the polymer layer and correspondingly generates larger interfacial electrostatic stress. When charge relaxation time is much shorter than processing time ($\boldsymbol{S} >> 1$, $\boldsymbol{S}$ represents the ratio of a time scale for free charge conduction to the process time scale, $S = \sigma_p \eta \gamma d^3 / \varepsilon_0^3 U^4$, where $\sigma_p$ and $\eta$ are conductivity and viscosity of the polymer layer, respectively), the characteristic wavelength $\lambda$ is given by Equation 2,

$$\lambda_{\max} = \frac{2\pi}{U}\sqrt{\frac{2\gamma}{\varepsilon_0}}(d-h)^{\frac{3}{2}} \quad (2)$$

Given its high dimensionless conductivity ($\boldsymbol{S} \approx 10^4$), the EHDP material system with $\varphi_{P/B} = 0.05$ has a theoretical $\lambda$ of 150 μm that calculated by Equation 2 on the basis of the leaky dielectric model. In spite of a slight mismatch between theoretical and experimental values especially from the perfect dielectric model, the results herein demonstrate convincing experimental distinction between the ‘‘perfect’’ and ‘‘leaky’’

dielectric models. Leaky dielectric material exhibits smaller characteristic wavelength than perfect dielectric material in EHDP patterning, which is consistent with theoretical predictions.

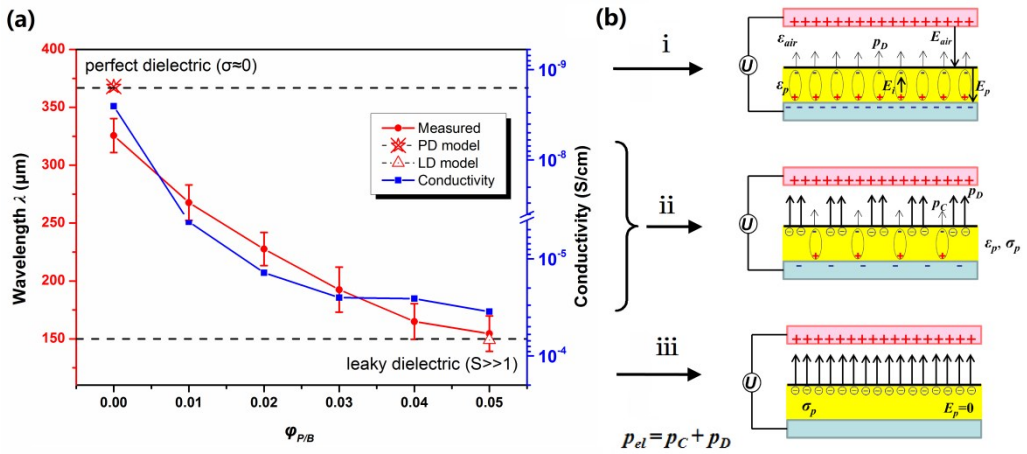


**Figure S3.** a) Variation in wavelength of EISF patterns and the conductivity of raw materials as function of PMAEPy content $\varphi_{P/B}$; b) Schematic of the origin of the electrostatic forces at the film-air interface. The polarization (i: $\varphi_{P/B}$=0.00, $\sigma_p \approx 0$, $E_{p[\varphi P/B=0.00]}>0$) or the accumulation of free charges (iii: $\varphi_{P/B} \geqslant 0.05$, $S>>1$, $\sigma_p>0$, $E_{p[\varphi P/B \geq 0.05]}=0$) or both of two effects(ii: $0<\varphi_{P/B}<0.05$, $\sigma_p>0$, $0<E_{p[0<\varphi P/B<0.05]}<E_{p[\varphi P/B=0.00]}$) of the film leads to an effective surface charge density, yielding an attractive interaction between the charges at the polymer-air interface with the opposite charges at the upper electrode.

It is noteworthy that the theoretical $\lambda$ calculated by Equation (2) is the minimum value under the given EHDP condition ($h$ = 13 μm, $d$ = 28 μm, $f$ = 0.464, and $U$ = 200V). For a leaky dielectric material system ($\varphi_{P/B}>0$), the charges at polymer-air interface under electric field are composed of polarized charges and free charges [as shown in Figure S3(b-ii)]. Compared to perfect dielectric, the introduction of free space charges in leaky dielectric will increase the electrostatic driving pressure $p_{el}$ by firstly offering an additional pressure, i.e., Coulomb pressure ($p_C$), in EISF process and secondly enhancing the dielectric pressure $p_D$ through inner electric field shielding.[5] With the

increase of $\varphi_{P/B}$, namely the increase of conductivity, free charges become dominant thereby enhance interfacial electrostatic destabilizing stress that drive EHD pattern formation. With relatively high conductivity ($S >> 1$), charge conduction is much faster compared to motion of the interface, the characteristic wavelength $\lambda$ is neither relevant to conductivity nor dielectric constant of the EHDP material system. Under such circumstance, available charges at polymer-air interface are solely accumulated free charges and there is no electric field inside the film [Figure S3(b-iii)]. There would be no additional reduction in characteristic wavelength of EHDP patterning with further increase of material conductivity ($\varphi_{P/B} > 0.05$).

**Table S1.** Physical properties of PMAEPy/BPAEODMA EHDP material systems and corresponding EHDP time scale.

| $\varphi_{P/B}$ | Viscosity [mPa·s][a)] | Conductivity [S/cm][b)] | Dielectric constant[c)] | Surface tension [mN/m] | $t_f$ [s] |
|---|---|---|---|---|---|
| 0.00 | 4.45 | $2.54\times10^{-9}$ | 2.61 | 29.0 | 5 |
| 0.05 | 5.08 | $3.50\times10^{-5}$ | 24.5 | 29.7 | <<1 |

[a)] The viscosity data was measured at shear rate of 100 $s^{-1}$; [b)] the conductivity was acquired at 10 Hz to match the low-frequency (or DC) electric field applied during EHDP; [c)] the dielectric constant of low-conductivity material ($\varphi_{P/B} = 0.00$) was also obtained at 10 Hz, whereas the dielectric constant of high-conductivity material ($\varphi_{P/B} = 0.05$) was acquired at a higher frequency (1 MHz) to minimize measurement error caused by the masking effect of electrode polarization.[6,7] All the results were obtained from EHDP systems containing 30 wt.% PMAEPy/BPAEODMA at 30 °C.

## 4. Static Water Contact Angle on Flat and Patterned Films

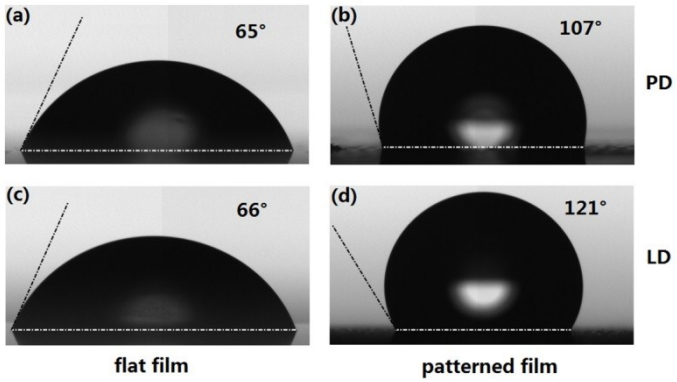


**Figure S4.** Static Water contact angles on the solid films prepared from perfect dielectric (a, b; $\varphi_{P/B} = 0.00$) and leaky dielectric material (c, d; $\varphi_{P/B} = 0.05$). (a) and (c) involve flat films, while (b) and (d) involve patterned films with EISF structures on surface as shown in Figure S2 a and f, respectively.

As seen in Figure S4, the solid flat films prepared from perfect dielectric ($\varphi_{P/B} = 0.00$) and leaky dielectric ($\varphi_{P/B} = 0.05$) have hydrophilic surface and show similar water contact angle of about 65°, probably indicating that the incorporation of PMAEPy won't affect the surface characteristic of flat films. In contrast, the films with EISF patterns prepared from perfect dielectric and leaky dielectric material both show hydrophobic feature and have contact angles of 107° (64 % increment from the value of the flat surface) and 121° (83 % increment from the value of the flat surface), respectively. For the films prepared from same material, the increase in contact angle shows the importance of contact area modification resulting from the addition of a surface pattern. According to Cassie wetting theories,[8,9] the calculated effective contact angle of the films with patterned surface from perfect dielectric [shown in Figure S2(a)] and leaky dielectric material [shown in Figure S2(f)] were 114° and 132°, respectively. These values are quite similar to the observed contact angles of the patterned surface. Therefore, it is reasonable to assume that the hydrophobicity

wetting state of the patterned surface is a result of Cassie wetting mechanism. As the patterns films prepared from perfect dielectric and leaky dielectric material share the same EISF process and parameters, the difference in hydrophobicity definitely stems from their different material properties. Leaky dielectric has higher dielectric constant and conductivity when compared with perfect dielectric, which yield dense pillars (reduced characteristic wavelength) with smaller diameters, thereby resulting in higher hydrophobicity.

## 5. Microstructures Derived from DEP-ECF DI Process without Applying Voltage

As seen in Figure S5, both the perfect and leaky dielectric materials exhibited rather low filling height of about 1~2 μm that driven only by natural capillary force when no voltage is applied. By contrast, much higher filling height (at least 7.5 μm) can be fulfilled by applying a voltage of 200V. The comparison of the results confirms that the DEP-ECF force does play a critical role in overcoming the trap air to pull resist into high-depth cavities.

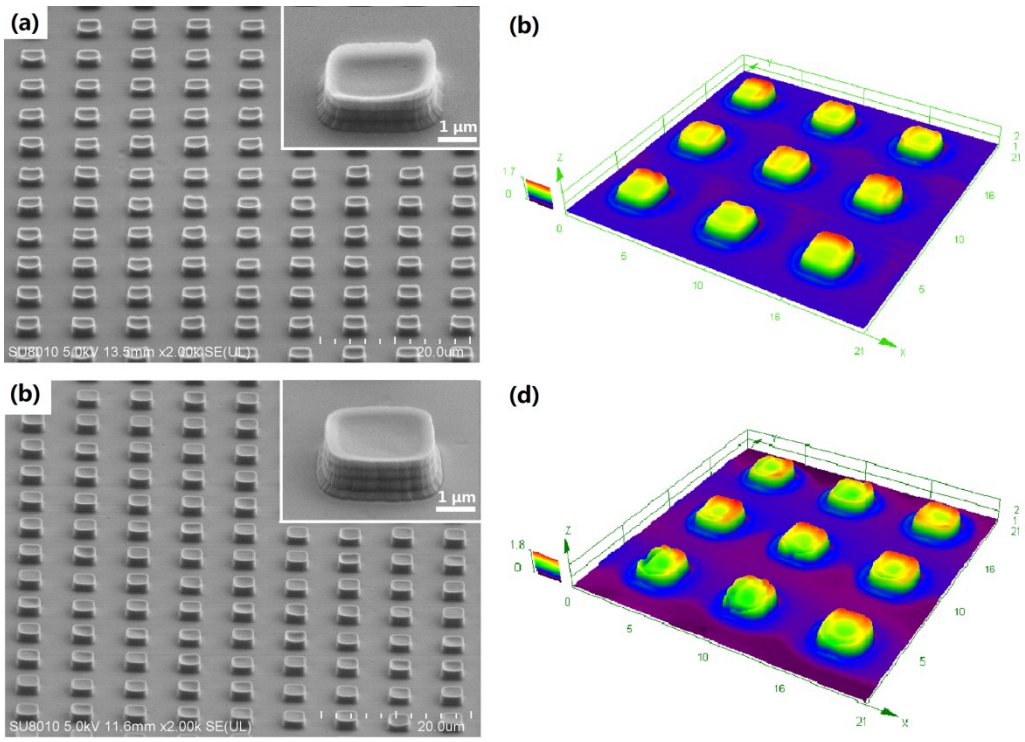


**Figure S5.** SEM images and the corresponding 3D images of microstructures fabricated using the same process and template as DEP-ECF DI but with no voltage applied. (a, b) perfect dielectric materials ($\varphi_{P/B} = 0.00$) and (c, d) leaky dielectric material ($\varphi_{P/B} = 0.05$).

## 5. Quasi-electrowetting by DEP-ECF Force

Quasi-electrowetting experiment has been successfully employed to demonstrate the existence of DEP-ECF acting on the three-phase contact line (TCL).[10,11] Figure S6 depicts the experiment of quasi-electrowetting by DEP-ECF force. In this experiment, a compound liquid droplet (about 5 μL) was dripped on the FAS-treated $SiO_2$/Si plane electrode, and a conductive needle (Pt) with the diameter of 0.45 mm was then immersed into the droplet which sat on the FAS-treated $SiO_2$/Si plane electrode at a distance of 0.5 mm from the needle end to the $SiO_2$/Si plane. The needle electrode was connected to high voltage (10 Hz-square-wave voltage, $U$, ranging from 0 V to 500 $V_{pp}$) and the FAS-treated $SiO_2$/Si plane electrode was grounded (see Figure S5).

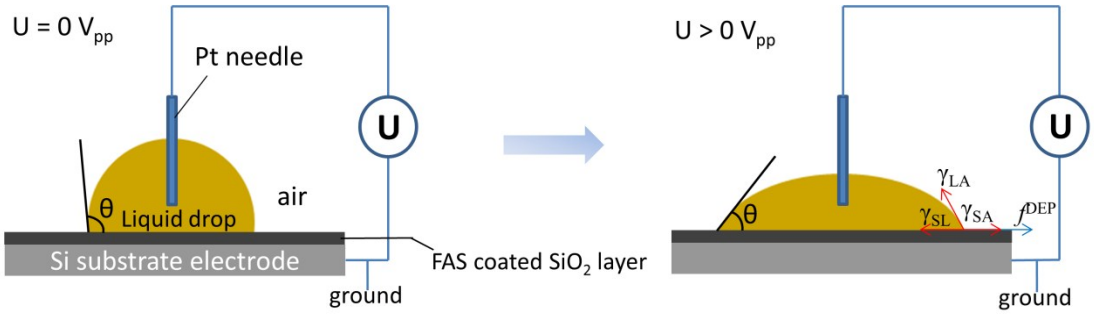


**Figure S6.** Schematic illustration for quasi-electrowetting by DEP-ECF force.

Figure S7 exhibits the contact angle (or wetting angle) variation by applying the voltage. It is clearly seen that the contact angle reduce when the voltage is exerted on the liquid drop, revealing the existence of DEP-ECF acting on the three-phase contact line.[6] DEP-ECF force can drive liquid to spread around on the $SiO_2$ surface, and thus reduce the wetting angle. Fundamentally, the DEP-ECF force derives from the comprehensive effect of liquid dielectrophoresis (L-DEP) generated pressure ($p^{DEP}$, a specific form of electrohydrodynamic pressure) and Laplace pressure. The electrohydrodynamic force can formulated in terms of the Korteweg-Helmholtz force,[12]

$$\vec{f}_e = \rho_f \vec{E} - \frac{1}{2} E^2 \nabla \varepsilon \qquad (3)$$

where $\rho_f$ is the density of free charges within the liquid, $E$ is the electric field strength, and $\varepsilon$ is the permittivity of liquid. The first term on the right side is the Coulombic force exerted on free charges, and the second terms on the right-hand side is the polarization force exerted on the dipoles, respectively. The Laplace pressure $p_L$ can be given by

$$p_L = \frac{2\gamma_{LA}}{r} \qquad (4)$$

where $\gamma_{LA}$ and $r$ respectively refer to the surface tension coefficient and the curvature radius of the liquid/air interface. Figure 2d has depicted that the surface tensions keep unchanged with increasing the PMAEPy content, and thus the Laplace pressure would

keep constant as long as the curvature radius are fixed. Obviously, the DEP-ECF force is governed by the exerted electric field as well as the electrical properties (i.e., $\sigma$ and $\varepsilon$) according to Eq.(3). For both the perfect dielectric and leaky dielectric material, the DEP-ECF force increase with increasing of the applied voltage, thereby leading to a reduction in contact angle (shown in Figure S7).

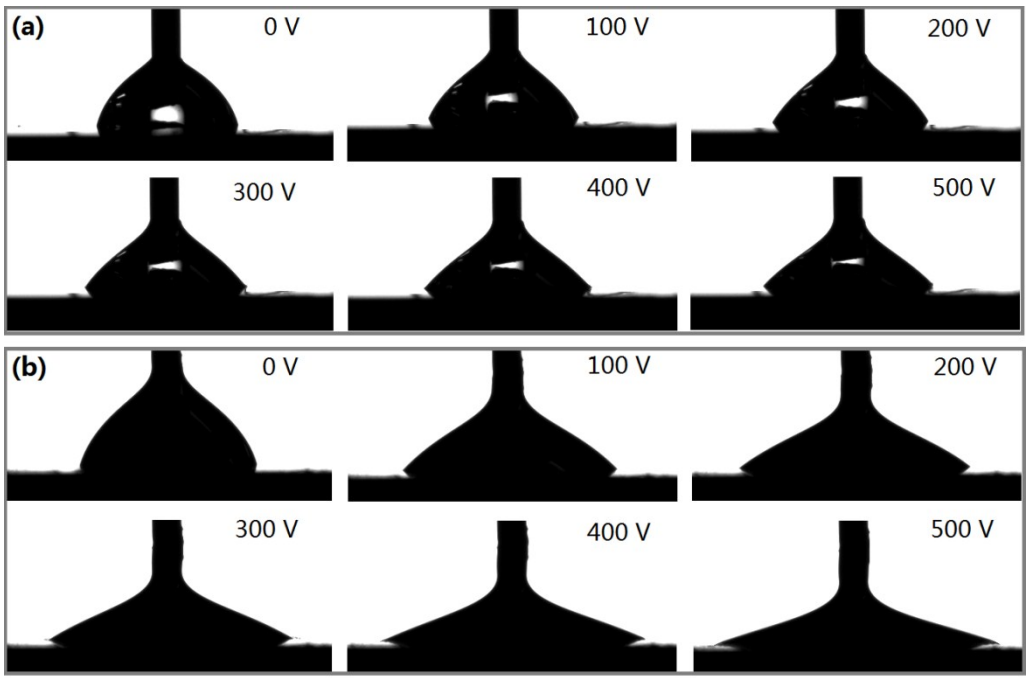


**Figure S7.** Influence of an increasing voltage on the contact angle $\theta$ (CA) of (a) perfect dielectric liquid material ($\varphi_{P/B}$ = 0.00) and (b) leaky dielectric liquid material ($\varphi_{P/B}$ = 0.05) on the FAS-treated $SiO_2$/Si plane substrate.

Figure S8 shows the comparison of quasi-electrowetting between perfect dielectric and leaky dielectric droplet by DEP-ECF. It can be seen that both perfect dielectric and leaky dielectric have contact angle around 72° with no voltage applied. After applying the same voltage of 200 V, the contact angle of perfect dielectric decreases to 55°, whereas the contact angle of leaky dielectric has a more significant reduction to 34°. Such difference in contact angle can be ascribed to the higher DEP-ECF force

of leaky dielectric which is the contribution from both the higher $\sigma$ and $\varepsilon$ when compared to its perfect dielectric counterpart.

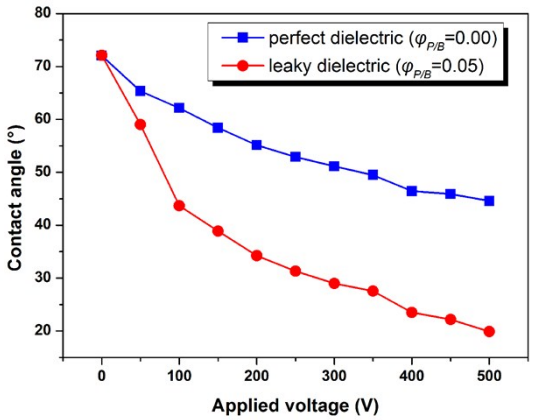


**Figure S8.** Comparison between experimental results for quasi-electrowetting of perfect dielectric and leaky dielectric droplet by DEP-ECF.

## References


(1) Li, X.; Tian, H.; Shao, J.; Ding, Y.; Liu, H. *Langmuir* **2013**, *29*, 1351–1355.

(2) Schäffer, E.; Thuran-Albrecht, T.; Russell, T. P.; Steiner, U. *Europhys. Lett.* **2001**, *53*, 518–524.

(3) Pease III, L. F.; Russel, W. B. *J. Nonnewton. Fluid Mech.* **2002**, *102*, 233–250.

(4) Pease, L. F.; Russel, W. B. *J. Chem. Phys.* **2003**, *118*, 3790.

(5) Tian, H.; Wang, C.; Shao, J.; Ding, Y.; Li, X. *Langmuir* **2014**, *30*, 12654–12663.

(6) Wu, H.; Zhao, K. *Langmuir* **2015**, *31*, 8566–8576.

(7) Fan, X.; Zhao, K. *Soft Matter* **2014**, *10*, 3259–3270.

(8) McDonald, B.; Shahsavan, H.; Zhao, B. *Macromol. Mater. Eng.* **2014**, *299*, 237–247.

(9) Liu, K.; Yao, X.; Jiang, L. *Chem. Soc. Rev.* **2010**, *39*, 3240–3255.

(10) Li, X.; Shao, J.; Tian, H.; Ding, Y.; Li, X. *J Micromech. Microeng.* **2011**, *21*, 065010.

(11) Tian, H.; Shao, J.; Ding, Y.; Li, X.; Liu, H. *Langmuir* **2013**, *29*, 4703–4714.

(12) Jones, T. B. *Langmuir* **2002**, *18*, 4437–4443.